



**HAL**  
open science

## On the design of conical hoppers for spent coffee grounds: Moisture content and particle-size effects

L. Massaro Sousa, C.G. G Schulz, R. Condotta, M.C. C Ferreira

### ► To cite this version:

L. Massaro Sousa, C.G. G Schulz, R. Condotta, M.C. C Ferreira. On the design of conical hoppers for spent coffee grounds: Moisture content and particle-size effects. *Journal of Food Engineering*, 2021, 300, pp.110537. 10.1016/j.jfoodeng.2021.110537 . hal-03150765

**HAL Id: hal-03150765**

**<https://ifp.hal.science/hal-03150765>**

Submitted on 24 Feb 2021

**HAL** is a multi-disciplinary open access archive for the deposit and dissemination of scientific research documents, whether they are published or not. The documents may come from teaching and research institutions in France or abroad, or from public or private research centers.

L'archive ouverte pluridisciplinaire **HAL**, est destinée au dépôt et à la diffusion de documents scientifiques de niveau recherche, publiés ou non, émanant des établissements d'enseignement et de recherche français ou étrangers, des laboratoires publics ou privés.

1 An accepted manuscript in Journal of Food Engineering

2 (DOI: 10.1016/j.jfoodeng.2021.110537, Vol. 300, July 2021, Article No 110357, 8 p..)

3  
4  
5 **On the Design of Conical Hoppers for Spent Coffee Grounds:**  
6 **Moisture Content and Particle-Size Effects**

7 **L. Massaro Sousa<sup>13\*</sup>, C. G. Schulz<sup>2</sup>, R. Condotta<sup>2</sup>, and M. C. Ferreira<sup>3</sup>.**

8  
9  
10 <sup>1</sup>Process Design and Modeling Division, IFP Energies Nouvelles,  
11 Rond-Point Échangeur de Solaize, 69360 Solaize, France

12 <sup>2</sup>Chemical Engineering Department, Centro Universitário FEI, Av. Humberto de Alencar  
13 Castelo Branco 3972, 09850-901, São Bernardo do Campo, Brazil

14 <sup>3</sup>Drying Center for Pastes, Suspensions, and Seeds, Chemical Engineering Department,  
15 Federal University of São Carlos, P.O. Box 676, 13565-905, São Carlos, Brazil

---

\* Corresponding author. E-mail address: lucas.massaro-sousa@ifpen.fr (L. Massaro Sousa).

16

## ABSTRACT

17 Spent coffee ground (SCG) is a food waste with promising potential for reuse in pilot-  
18 to-industrial scale processes provided that storage and handling issues are overcome. Here  
19 some key bulk and flow properties of SCGs were determined with FT4 rheometer, for  
20 powders with different particle-size distribution ( $249.1 \leq d_v \leq 583.1 \mu\text{m}$ ) and moisture content  
21 ( $2.8\% \leq MC \leq 62.5\%$ ). These properties were used to evaluate the design of mass-flow silo  
22 hoppers following the classical Jenike theory. The SCGs flowability worsened by decreasing  
23  $d_v$  and increasing  $MC$ , with indexes between  $1.09 \leq HR \leq 1.92$  and  $2.5 \leq FF \leq 15.0$ . The minimum  
24 hopper inclination and outlet diameter ranged from  $9.9^\circ$  to  $17.1^\circ$  and 0.40 to 1.00 m. A  
25 sensitivity analysis for the hopper design was performed, and a densification equation was  
26 coupled to Jenike's method to ease future hopper designs for SCGs with different properties.  
27 Ultimately, the results showed that careful consideration must be given to  $d_v$  and  $MC$  to  
28 design effective devices to handle SCGs.

29 **Keywords:** biomass, silo, rheometer, powder handling, Jenike.

## 30 **1 Introduction**

31 Coffee, which is an agricultural product with distinguished taste and aroma, is widely  
32 used as an ingredient in the food, pharmaceutical, and cosmetic industries, as well as  
33 consumed as a beverage. It is a commodity traditionally produced in emerging countries, such  
34 as Brazil, Colombia, and Vietnam, that generated combined revenue of around US\$ 11 billion  
35 in 2019, which is a major contribution to the countries' trade market (Voorra et al., 2019).  
36 Over the last decade, global coffee consumption has increased by around 2% annually,  
37 reaching almost 10 million tonnes in 2019 (International Coffee Organization, 2019). Owing  
38 to the expected growth of the world's population by 25% until 2050, from 7.7 to 9.7 billion  
39 people (United Nations, 2019), coffee is likely to play an even bigger role in the coming  
40 decades.

41 Almost 50% of global coffee production is processed for instant coffee making  
42 (Mussatto et al., 2011). In the soluble coffee industry, coffee fruit and beans are initially  
43 processed into roasted coffee through some separation, drying, milling, and roasting steps,  
44 and then soluble coffee powder is obtained from steaming extraction and spray-drying  
45 (McNutt and He, 2019; Silva et al., 1998). Spent Coffee Ground (SCG) is the main solid  
46 residue generated in this process, at a rate of 2.5 million tons per year. It has a low ash  
47 content, and a high heating value similar to that of coal (25 kJ/kg) (Massaro Sousa and  
48 Ferreira, 2019a). These characteristics allow using SCG powders to generate renewable  
49 energy and steam within the industry, hence contributing to an attractive energy balance in  
50 this process.

51 A general search in the Science Direct database shows that to date, about 1,000 research  
52 papers have been published focusing on SCGs, with a significant increase of interest in this  
53 topic recently, as the rate of publication has grown from 2 papers/year back in the 90s to  
54 about 250 papers in 2020. Overall, these papers focused on reporting physico-chemical

55 properties for spent coffee grounds (Ballesteros et al., 2014; Massaro Sousa and Ferreira,  
56 2019b; Mussatto et al., 2011; Silva et al., 1998) and on a wide variety of applications,  
57 including drying and dewatering (Gómez-de la Cruz et al., 2015; Rocha et al., 2021; Tun et  
58 al., 2020), feeding of reactors (Massaro Sousa et al., 2020a, 2020b; Massaro Sousa and  
59 Ferreira, 2020a), solid-state fermentation (Murthy and Naidu, 2012), production of biofuels  
60 (Al-Hamamre et al., 2012; Kondamudi et al., 2008), extraction of bioactive and antioxidant  
61 compounds (Ballesteros et al., 2017; Brazinha et al., 2015; Karmee, 2018), preparing  
62 biopolymeric films for food packaging (Coelho et al., 2021; Thiagamani et al., 2017),  
63 combustion, gasification, and pyrolysis (Campos-Vega et al., 2015; Kelkar et al., 2015;  
64 McNutt and He, 2019; Silva et al., 1998) and so on.

65         Some key bottlenecks for implementing the previous applications on the pilot and  
66 industrial levels are related to the storage and handling of SCGs throughout the units. For  
67 instance, it is paramount to design silos with a stable discharge of solids at predictable flow  
68 rates, so that they can be used as reliable solid feeders or as intermediary/storage vessels to  
69 suppress eventual process instabilities (Barletta et al., 2015; Dai et al., 2012; Ilic et al., 2018;  
70 Ramírez-Gómez, 2016). While trial-and-error methods can be used for this design, the results  
71 are often disappointing, with the presence of dead zones of solids within the hopper or no  
72 solids flow out of the silo. Moreover, in the case of biomass residues such as SCGs, the  
73 particle-size distribution, moisture content, and flow attributes vary due to the processing,  
74 thus enhancing the difficulties associated with these solids' handling and hopper design.

75         Recently, some physical and flow properties of dry and moist SCG samples have been  
76 determined for the basic understanding of SCGs flowability and compressibility (i.e. repose  
77 angle, Hausner ratio, and bulk density) (Massaro Sousa and Ferreira, 2019a, 2019b).  
78 However, there is still a gap in knowledge concerning the measurement of flow properties for  
79 SCGs with shearing cells, and on using these properties for equipment design.

80 Therefore, this paper is aimed at understanding the flow pattern of industrial food waste  
81 with promising potential for reuse, as well as assisting its storage and handling. First, some  
82 key physical and flow properties of SCGs with different particle-size distribution and  
83 moisture content were measured with a rheometer. Then, these properties were used to  
84 investigate the design of silo hoppers for the effective mass-flow discharge of powders.

## 85 **2 Material and Methods**

### 86 **2.1 Materials**

87 The SCG samples were prepared by brewing a commercial blend of Arabica and  
88 Robusta grains (Três Corações, São Carlos-SP, Brazil). The powders were oven-dried at  
89  $105\pm 2$  °C for 24 h and sieved into three base samples named  $A_{100}$ ,  $B_{100}$ ,  $C_{100}$ . Sample  $A_{100}$  has  
90 a particle-size distribution between 600 and 500  $\mu\text{m}$ , while the size of sample  $B_{100}$  ranges  
91 from 500 and 300  $\mu\text{m}$ , and  $C_{100}$  lies between 300 and 150  $\mu\text{m}$ .

92 Additional dry samples were prepared by mixing the coarser samples with the finest one  
93 ( $C_{100}$ ) in a percentage of 10% and 20% in mass, originating samples  $A_{90}C_{10}$ ,  $A_{80}C_{20}$ ,  $B_{90}C_{10}$ ,  
94 and  $B_{80}C_{20}$ . Finally, the base samples were humidified to 20% and 60% on a wet basis by  
95 adding water in a glass flask, which was sealed and stored at 4 °C for 60 h. After every 24 h,  
96 the flask was opened and the powder was homogenized to ensure uniform water distribution.  
97 The moist samples are designated  $A_{100}^{20\%}$ ,  $A_{100}^{60\%}$ ,  $B_{100}^{20\%}$ ,  $B_{100}^{60\%}$ ,  $C_{100}^{20\%}$ , and  $C_{100}^{60\%}$ .

98 As previously mentioned, a total of seven dry and six moist SCG powders were  
99 prepared, aiming at understanding the effect of samples' size and moisture content on SCG  
100 flow properties, densification kinetics, and silo hopper design. These samples were selected to  
101 cover a wide range of powder properties that are commonly observed in the industrial  
102 processing of this biomass waste (Silva et al., 1998).

103 2.2 Characterization of SCGs properties

104 Particle-size distribution and mean diameter (De Brouckere diameter -  $d_v$ ) of the dry  
105 samples was measured, in duplicate, by laser diffraction technique using BlueWave model  
106 equipment (MicroTrac, Pennsylvania, USA) with air as dispersion media. Particle sizes from  
107 0.01 to 2,800 microns can be accurately measured with this equipment, which covers the size  
108 range for the SCGs.

109 Moisture content ( $MC$ ) of SCG samples was measured with an infrared drying balance  
110 model IV-2000 (Gehaka, São Paulo, Brazil) in duplicate. The moisture contents are reported  
111 in wet basis.

112 Bulk density of the samples was evaluated under different normal pressures ( $N$ ) applied  
113 to the powder bed in an FT4 rheometer (Freeman Technology, Tewkesbury, UK). First, a  
114 known quantity of SCGs is conditioned on the rheometer and based on the volume occupied  
115 by the powders, the loose bulk density ( $\rho_{bl}$ ) is determined. Then, normal pressures of 0.5, 1, 2,  
116 4, 6, 8, 10, 12, and 15 kPa are sequentially applied with a vented piston that allows air to  
117 escape from the bed out of the vessel during compression. The reduction of powders volume  
118 is measured, and the bulk density at each  $N$  is obtained. The Hausner ratio ( $HR$ ) is calculated  
119 from the ratio of the consolidated bulk density measured at 15 kPa ( $\rho_{bc}$ ) and  $\rho_{bl}$ , as proposed  
120 by (Baião et al., 2018).

121 2.3 Granular shear and wall friction measurements

122 Powder shear and wall friction measurements were performed in an FT4 rheometer with  
123 shear cell accessory: 50 mm of internal diameter and 85 cm<sup>3</sup> in volume vessel, a 48 mm shear  
124 head diameter and 48 mm diameter disc of stainless steel. The SCG sample was initially  
125 homogenized and pre-consolidated within the rheometer by the standard procedure of the  
126 equipment, allowing air to escape from the bed out of the vessel in the pre-consolidation  
127 stage. After, pre-shear was performed at normal consolidation stresses of 15, 9, 6, and 3 kPa,

128 followed by a shear step to estimate incipient failure (of the consolidated sample) at 5  
129 different normal stress conditions induced in the powder bed for each level of consolidation,  
130 according to ASTM D7891-15 (American Society for Testing Material, 2015). The assays  
131 were performed in duplicate for all SCG samples.

132 From this experiment, the yield locus and effective yield locus are obtained. By plotting  
133 the Mohr circles, some flow parameters for the powders are determined, such as cohesion ( $c$ ),  
134 angle of internal friction ( $\sigma$ ), effective angle of internal friction ( $\delta$ ), unconfined yield strength  
135 ( $UYS$ ), major consolidating stress ( $MCS$ ), and flow function ( $FF$ ). The  $FF$  is obtained from  
136 the ratio of  $UYS$  to  $MCS$  and is used as a parameter to describe the strength of a bulk solid.  
137 Depending on  $FF$ , the powder flowability is classified as *free-flowing* ( $FF \geq 10$ ), *easy-flowing*  
138 ( $4 \leq FF < 10$ ), *cohesive* ( $2 \leq FF < 4$ ), *very cohesive* ( $1 \leq FF < 2$ ), or *not flowing* ( $FF < 1$ ).

139 Finally, the wall friction angle ( $\phi_w$ ) of the powders was estimated by measuring  
140 frictional resistance between a metallic disc and SCG samples under consolidation stress  
141 from 3 to 15 kPa, in duplicate. The disc is made of stainless steel, which is a material  
142 commonly used in the food industry hoppers.

#### 143 2.4 Conical hopper design

144 Design of the conical hopper for mass-flow discharge consists of using the measured  
145 flow properties with the rheometer for determining the minimum hopper half-angle ( $\theta_m$ ), and  
146 minimum hopper outlet size ( $D_m$ ). In this way,  $\theta_m$  is calculated according to (Oginni and  
147 Fasina, 2018):

$$\theta_m = 90^\circ - 0.5 \cos^{-1}[(1 - \sin \delta)/2 \sin \delta] - \beta \quad (1)$$

$$\beta = [\phi_w + \sin^{-1}(\sin \phi_w / \sin \delta)]/2 \quad (2)$$

148 After calculating  $\theta_m$  from Eqs. (1) and (2), it is recommended to adopt a margin of  
149 safety for  $\theta_m$  to allow for differences in the wall surfaces or slight variations in the bulk solid



150 properties, then the angle should be reduced by 3°. The minimum hopper outlet size is  
 151 calculated by (Oginni and Fasina, 2018):

$$D_m = H(\theta_m)\sigma_{cr}/(\rho_b g) \quad (3)$$

$$H(\theta_m) = (130 + \theta_m)/65 \quad (4)$$

152 The critical applied stress ( $\sigma_{cr}$ ) represents the limiting value of the unconfined yield  
 153 strength at which a stable arch can be formed. This value can be obtained from the  
 154 intersection of the powder flow function ( $FF$ ) with the hopper flow factor line ( $ff$ ) in a graph  
 155 of the major consolidation stress (x-axis) versus the unconfined yield stress (y-axis). Note that  
 156  $ff$  is a straight-line through the origin with a slope equal to the inverse of  $ff$  (Fitzpatrick et al.,  
 157 2004).

158 Although  $ff$  can be obtained from the design charts shown in Jenike's famous Bulletin  
 159 163 (Jenike, 1964), algebraic expressions derived from these charts are preferred as they can  
 160 be readily implemented in spreadsheets (Arnold and McLean, 1976; Condotta, 2017; Enstad,  
 161 1975). The set of equations are shown below:

$$ff = Y(1 + \sin \delta)H(\theta_m)/[2(X - 1) \sin \theta_m] \quad (5)$$

$$X = 2 \sin \delta / (1 - \sin \delta) [1 + \sin(2\beta + \theta_m) / \sin \theta_m] \quad (6)$$

$$Y = (A + B) / C \quad (7)$$

$$A = 2[1 - \cos(\beta + \theta_m)] \sin \theta_m \quad (8)$$

$$B = \sin \beta \sin(\beta + \theta_m) \sin(\beta + \theta_m) \quad (9)$$

$$C = (1 - \sin \delta) \sin(\beta + \theta_m) \sin(\beta + \theta_m) \sin(\beta + \theta_m) \quad (10)$$

162 There are three possible scenarios concerning the intersection of  $FF$  and  $ff$  (in the  
 163 positive x-y quadrant) that might affect determining  $\sigma_{cr}$ , and consequently  $D_m$ :

164 i) if there is an intersection between  $FF$  and  $ff$ ,  $\sigma_{cr}$  is determined at the y-axis and used  
 165 to calculate  $D_m$  with Eq (3);

166 ii) if there is no intersection, and  $FF$  lies above  $ff$ , the powder does not flow under  
167 gravitational discharge or with the proposed hopper wall material;  
168 iii) if there is no intersection, and  $FF$  lies below  $ff$ , from the perspective of cohesive  
169 arch formation, the powder will flow with any  $D_m$  as the applied stress at the hopper  
170 outlet overcomes the unconfined yield strength of the arch. In this case, the  
171 minimum hopper outlet can be selected either to avoid interlocking effects (usually  
172  $D_m$  is 10 to 12 times the diameter of the largest particle (Oginni and Fasina, 2018))  
173 or by other non-standardized criteria based on the handling experience of specific  
174 powders or fitted correlations (Chen et al., 2012; Fitzpatrick et al., 2004; Salehi et  
175 al., 2019).

### 176 3 Results and Discussion

#### 177 3.1 Physical properties of SCGs

178 Some key properties of the SCG samples are presented in Table 1, such as the volume  
179 mean diameter, moisture content, as well as the loose and consolidated bulk densities  
180 measured under pressures of 0 and 15 kPa, respectively. Hausner ratio ( $HR=\rho_{bc}/\rho_{bl}$ ) is an  
181 important parameter often used for industrial quality control of pelletizing and feeding  
182 operations as it quantifies the flowability and compressibility of powders. Based on this  
183 parameter, the lower is the  $HR$ , the better is the flowability/compressibility of the sample,  
184 which generally means a lower likelihood of operational problems related to powders'  
185 handling.

186 It can be observed from Table 1 that the flowability of SCGs worsens as the moisture  
187 content increases and as the sample's mean diameter decreases. For example, the flowability  
188 of the dry and coarsest sample  $A_{100}$  is categorized as *excellent*, whereas the flowability of the  
189 finest sample  $C_{100}$  is categorized as *passable*. The  $HR$  of the dry powder mixtures are

190 intermediary to those of the base samples. Besides, the *HR* increases with the moisture  
 191 content, then the flowability of sample  $A_{100}^{60\%}$  is classified as *very poor*, while  $A_{100}^{20\%}$  is  
 192 *good*, for example. The effect of the moisture content and particle-size distribution on SCGs  
 193 flowability agree with previous literature results (Massaro Sousa and Ferreira, 2019a).

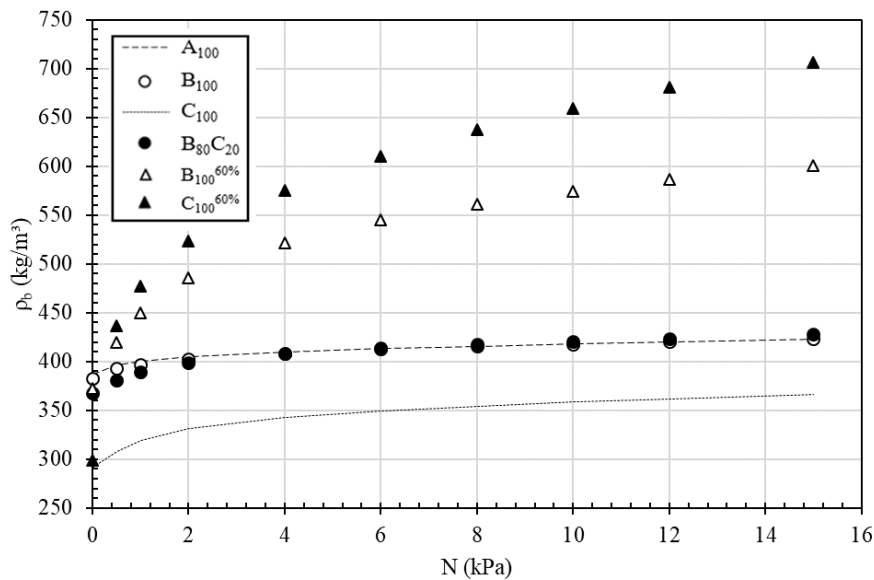
194 **Table 1.** Physical properties of spent coffee ground powders

SCG Sample	$d_V$ ( $\mu\text{m}$ )	MC (% w.b.)	$\rho_{bl}$ ( $\text{kg/m}^3$ )	$\rho_{bc}$ ( $\text{kg/m}^3$ )	HR (-)	Flowability classification
$A_{100}$	583.1	5.4	386	423	1.09	Excellent
$A_{100}^{20\%}$	-	25.1	368	436	1.18	Good
$A_{100}^{60\%}$	-	58.7	409	609	1.49	Very Poor
$B_{100}$	442.2	2.8	383	424	1.10	Excellent
$B_{100}^{20\%}$	-	21.4	367	443	1.20	Fair
$B_{100}^{60\%}$	-	62.5	373	610	1.64	Very, Very Poor
$C_{100}$	249.1	3.1	292	367	1.26	Passable
$C_{100}^{20\%}$	-	21.7	309	412	1.35	Poor
$C_{100}^{60\%}$	-	61.0	299	574	1.92	Very, Very Poor
$A_{90}C_{10}$	549.7	-	405	464	1.14	Good
$A_{80}C_{20}$	516.3	-	381	452	1.19	Fair
$B_{90}C_{10}$	422.9	-	372	424	1.14	Good
$B_{80}C_{20}$	403.6	-	368	428	1.16	Good

195 3.2 Densification kinetics of SCGs

196 Evolution of the powder bulk density with the applied pressure is known as the  
 197 densification curve, with initial and final points as the loose and consolidated bulk densities.  
 198 The values for  $\rho_{bl}$  and  $\rho_{bc}$  are presented in Table 1 for all SCG samples. The points and the  
 199 curvature of the densification curve depend on the bulk material and its properties, such as the  
 200 particle-size distribution, and moisture content. In this way, assessing the densification of  
 201 SCGs with different properties is crucial for the effective design and operation of units that  
 202 handle such biomass powders.

203 The effect of the particle-size distribution and moisture content on the densification  
 204 curves of SCGs is shown in Fig. 1. The dry samples exhibit similar densification patterns,  
 205 with a steep increase in the bulk density prior to  $N=4$  kPa, which represents around 70% of  
 206 the consolidated bulk density, and a nearly constant bulk density from  $N=10$  kPa onwards,  
 207 indicating that the maximum bed compaction has been achieved. More specifically, samples  
 208  $A_{100}$  and  $B_{100}$  have similar bulk densities, whereas the curve of the powder mixture  $B_{80}C_{20}$  is  
 209 slightly shifted downwards. Finally, the finest powder  $C_{100}$  has the lowest bulk density which  
 210 might be attributed to enhanced cohesion effects of van der Waals origin (Castellanos, 2005).



211 **Fig. 1.** Bulk density ( $\rho_b$ ) as a function of the applied normal stress for selected spent coffee  
 212 ground samples  
 213

214 Adding water to the dry samples increases the bulk density since air voids become  
 215 partially filled with water, which has a density thousand times greater than the air. For the wet  
 216 samples, there is a consistent increase in  $\rho_b$  with increasing  $N$ , and possibly the maximum bed  
 217 compaction has not been achieved at  $N=15$  kPa. In summary, the densification process is  
 218 slower for samples with higher cohesion, such as those containing finer particles or higher  
 219 moisture content. Although only a few SCG samples are shown in Fig. 1, the behavior  
 220 previously described covers all tested powders.

221 In a previous study (Massaro Sousa and Ferreira, 2019b), the densification of dry SCGs  
222 was assessed by tapping, which means that the powder bed is compacted with the bed weight  
223 and not by applying external forces. In general, powder beds 8% denser were achieved with  
224 tapping when compared to the applied pressure compaction, which can be attributed to: i) the  
225 facilitated rearrangement of particles in the voids promoted by the successive bed vibrations,  
226 and ii) limited range of the applied pressure to affect the compaction in the lower portions of  
227 the bed. From the practical perspective, these results highlight that for an accurate equipment  
228 design some assumptions on the powder densification mechanism should be performed  
229 beforehand, i.e., by considering the extent of variation of the bulk density within the  
230 equipment as a consequence of the applied normal pressures, and particles rearrangement due  
231 to vibration.

232 In the next section, an analysis is carried out to model the densification curves of SCGs.  
233 The aim is to use a single equation to describe the densification process with fitting  
234 parameters correlated to SCGs properties. In this way, the bulk density of a certain SCG  
235 sample can be readily estimated for a given  $N$ .

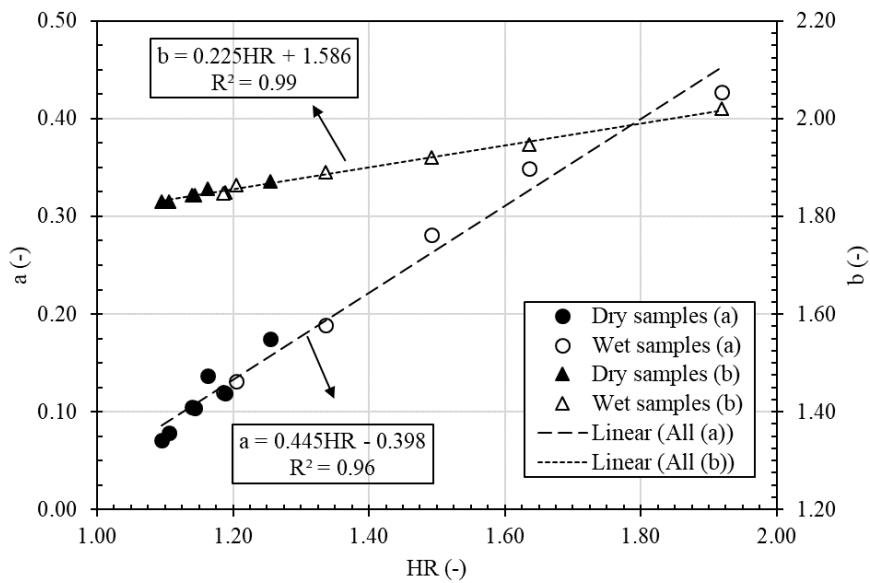
### 236 3.3 Modelling of SCGs densification

237 In a previous study, the two-parameter equation of Kawakita and Ludde (Eq. 11)  
238 (Kawakita and Lüdde, 1971) accurately predicted the densification curves of dry SCGs  
239 submitted to tapping. The parameters  $a$  and  $b$  of the equation could be correlated with the  
240 physical properties of the samples, such as the mean diameter and  $HR$  (Massaro Sousa and  
241 Ferreira, 2019b). Here, Eq. (11) is tested for predicting the densification behavior of dry and  
242 wet SCGs submitted to normal pressures. Since the relative density ( $D$ ) is the ratio of bulk to  
243 solid density ( $\rho_s=1,315 \text{ kg/m}^3$  for SCGs (Massaro Sousa and Ferreira, 2019a), the bulk density  
244 as a function of  $N$  can be explicitly calculated by Eq. (12).

$$(D - D_{bl})/D = abN/(bN + 1) \quad (11)$$

$$\rho_b = \rho_{bl}/[1 - abN/(bN + 1)] \quad (12)$$

245 The parameters  $a$  and  $b$  are shown in Fig. 2 as a function of the  $HR$  of the samples.  
 246 From Fig. 2, both parameters in Eq. (11) increase as  $HR$  rises. These findings are in line with  
 247 expectations since high  $HR$  indicates that powder bulk density changes significantly  
 248 throughout compaction, then high values for  $a$  and  $b$  are necessary to describe the steeper  
 249 variation on the kinetic curves of these powders.



250  
 251 **Fig. 2.** Parameters  $a$  and  $b$  as a function of the samples' Hausner ratio ( $HR$ )

252 Linear equations fitted the relationship between the parameters and  $HR$  accordingly  
 253 with regression coefficients of 0.99 and 0.96 for Eqs. (13) and (14), respectively. Also, the  
 254 data are randomly distributed around the lines of the fittings, which is evidence of non-biased  
 255 fittings.

$$a = 0.445HR - 0.398 \quad (13)$$

$$b = 0.225HR + 1.586 \quad (14)$$

256 By using Eqs. (12) to (14), it is possible to estimate the bulk density of SCGs for a  
 257 given  $N$  provided that both the  $HR$  and loose bulk density for the sample are known (see

258 Table 1). Difference between experimental and predicted values of bulk density is on an  
259 average of 24% in the range of  $0 \leq N \leq 15$  kPa. Nevertheless, we recommend using Eqs. (12)  
260 and (13) for predicting  $\rho_b$  over  $N \geq 2$  kPa as the mean differences lie below 13%. For  $N < 2$  kPa  
261 the differences reach 40% because the data become more dispersed as the loose bulk  
262 condition is approached.

263 From the above, information on SCGs bulk density can be readily obtained for various  
264 normal consolidation pressures, which is useful for equipment design and process control.

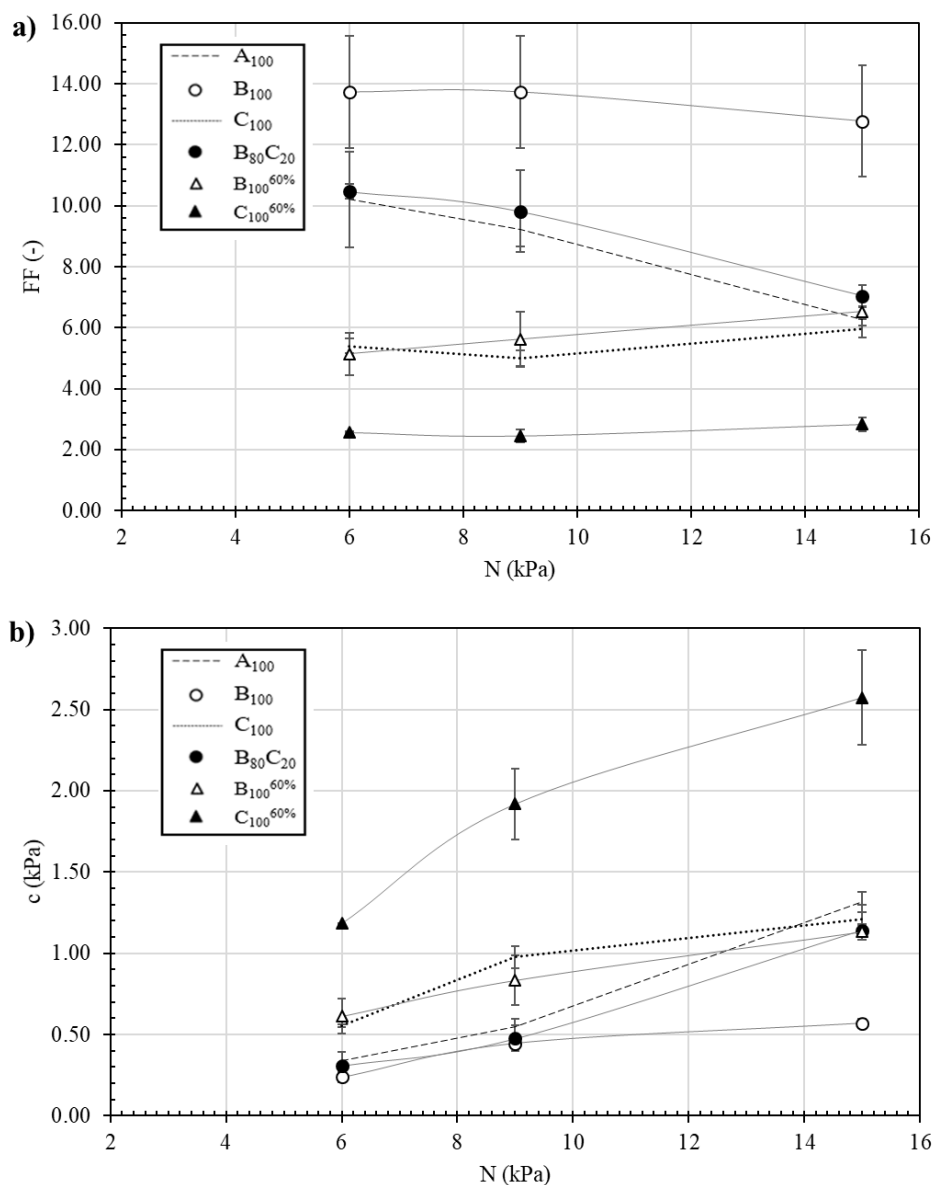
### 265 3.4 Flow properties of SCGs

266 In this section, the effect of the particle-size distribution and moisture content on the  
267 SCG flow properties measured with the FT4 rheometer is analysed. The flow function and  
268 cohesion of the powders are presented in Figures 3a and 3b, respectively, as a function of  $N$ .  
269 Overall, increasing the consolidation pressure leads to lower powder flow functions (Fig. 3a)  
270 and higher powder cohesion (Fig. 3b), as particle-particle contacts are enhanced within the  
271 rheometer under higher  $N$ .

272 Powders with higher  $FF$  have better flowability; hence, the sample with the finest  
273 particles ( $C_{100}$ ) has the worst flowability among the dry samples. This is due to the higher  
274 cohesion of this sample motivated by its greater specific surface area that enhances cohesive  
275 forces of van der Waals nature (Castellanos, 2005). Concerning the other dry powders, the  
276 flowability of sample  $A_{100}$  is worse than sample  $B_{100}$  probably due to particle-particle  
277 interlocking effects within the rheometer for the coarsest sample, whereas, intermediary  $FF$   
278 values are observed for the mixtures of coarse and fine particles.

279 By adding water to the dry SCG samples, cohesive forces of liquid bridge nature  
280 become important and powder flowability deteriorates as the moisture content increases. In  
281 Fig. 3a and 3b, for example, the wet sample  $B_{100}^{60\%}$  exhibits similar  $FF$  and cohesion than  
282 that of sample  $C_{100}$ , whereas sample  $C_{100}^{60\%}$  has the worst flowability among all SCG samples

283 due to a combined effect of liquid bridges and van der Waal interactions, since smaller  
 284 particles saturate its surface at reduced moisture content.



285

286

287 **Fig. 3.** Flow properties as a function of the consolidation stress for selected spent coffee  
 288 ground samples: a) flow function and b) cohesion

289

The previous conclusions concerning the *FF* and cohesion trends are also valid for the  
 290 SCG samples not shown in Fig. 3. The mean value of *FF* for all samples is presented in Table  
 291 2 along with the standard deviation and flowability classification. Although most of the  
 292 samples are categorized as *easy-flowing* powders with  $10 < FF < 4$ , it is noticeable that *FF*



293 decreases with increasing moisture content and with decreasing particle mean diameter,  
 294 leading to a *cohesive* behavior for sample C<sub>100</sub><sup>60%</sup>.

295 **Table 2.** Averaged values for SCG properties measured with the rheometer and flowability  
 296 classification

SCG Sample	$\delta$ (°)	$\phi_w$ (°)	FF (-)	Flowability classification
A <sub>100</sub>	40.3 ± 0.4 <sup>a</sup>	25.0 ± 2.0 <sup>a</sup>	9.0 ± 2.0 <sup>a</sup>	Easy flowing
A <sub>100</sub> <sup>20%</sup>	41.8 ± 0.5 <sup>b</sup>	27.5 ± 0.3 <sup>a</sup>	6.3 ± 0.9 <sup>b</sup>	Easy flowing
A <sub>100</sub> <sup>60%</sup>	42.5 ± 0.9 <sup>b</sup>	26.0 ± 1.0 <sup>a</sup>	6.0 ± 1.0 <sup>b</sup>	Easy flowing
B <sub>100</sub>	39.8 ± 0.4 <sup>a</sup>	25.0 ± 3.0 <sup>a</sup>	15.0 ± 4.0 <sup>c</sup>	Free flowing
B <sub>100</sub> <sup>20%</sup>	41.0 ± 0.8 <sup>ab</sup>	27.2 ± 0.5 <sup>a</sup>	8.0 ± 2.0 <sup>ab</sup>	Easy flowing
B <sub>100</sub> <sup>60%</sup>	43.1 ± 0.9 <sup>b</sup>	27.5 ± 0.6 <sup>a</sup>	5.0 ± 1.0 <sup>b</sup>	Easy flowing
C <sub>100</sub>	40.0 ± 0.7 <sup>a</sup>	27.0 ± 2.0 <sup>a</sup>	5.3 ± 0.5 <sup>b</sup>	Easy flowing
C <sub>100</sub> <sup>20%</sup>	40.9 ± 0.5 <sup>ab</sup>	28.8 ± 0.7 <sup>ab</sup>	5.1 ± 0.3 <sup>b</sup>	Easy flowing
C <sub>100</sub> <sup>60%</sup>	48.8 ± 0.9 <sup>c</sup>	30.8 ± 0.9 <sup>b</sup>	2.5 ± 0.2 <sup>d</sup>	Cohesive
A <sub>90</sub> C <sub>10</sub>	40.9 ± 0.7 <sup>ab</sup>	24.0 ± 3.0 <sup>a</sup>	8.0 ± 2.0 <sup>ab</sup>	Easy flowing
A <sub>80</sub> C <sub>20</sub>	41.1 ± 0.6 <sup>ab</sup>	25.0 ± 2.0 <sup>a</sup>	6.9 ± 0.8 <sup>ab</sup>	Easy flowing
B <sub>90</sub> C <sub>10</sub>	40.2 ± 0.4 <sup>a</sup>	26.0 ± 2.0 <sup>a</sup>	8.0 ± 2.0 <sup>ab</sup>	Easy flowing
B <sub>80</sub> C <sub>20</sub>	39.8 ± 0.5 <sup>a</sup>	25.0 ± 2.0 <sup>a</sup>	9.0 ± 2.0 <sup>a</sup>	Easy flowing

297 \* Values with different letters in the same column are significantly different at the 0.05 significance level

298 The average values for the effective angle of internal friction ( $\delta$ ) and wall friction angle  
 299 ( $\phi_w$ ) are presented in Table 2 along with their standard deviation, measured between  $N=3$  and  
 300 15 kPa. Similar to the cohesion and  $FF$ , both angles vary when  $N$  changes from 3 to 15 kPa:  
 301 while  $\delta$  exhibits a slight increase as  $N$  rises,  $\phi_w$  decreases with increasing  $N$ . Besides,  $\delta$  and  $\phi_w$   
 302 increases as the SCGs flowability worsens, i.e., with decreasing particle size and increasing  
 303 moisture content. These trends agree with results from the literature (Marinelli and Carson,  
 304 1992).

305 In practice, a minor worsening of powder flow attributes may compromise the operation  
 306 of various types of industrial equipment, such as those for the feeding and storing of solids.

307 Some evidence of the effect of powder flowability on the solid feeder's performance has been  
308 previously assessed in handling dry and moist SCGs to reactors with L-valve and spouted bed  
309 feeding devices (Massaro Sousa and Ferreira, 2020a, 2020b). The results of  $HR$  and  $FF$   
310 showed in Table 1 and Table 2 indicate that both indices are sensitive to the SCG size and  
311 moisture content; hence they might be useful for process monitoring and control.

312 In the next section, the design of silo hoppers is addressed aiming at an effective mass-  
313 flow discharge of SCGs with different properties. Apart from the bulk density (Sections 3.2  
314 and 3.3), the effective angle of internal friction ( $\delta$ ) and wall friction angle ( $\phi_w$ ) shown in Table  
315 2 are the properties used for the design of hoppers according to the classical Jenike theory.

### 316 3.5 Hopper design for SCGs

317 In the design of conical hoppers for mass-flow discharge, the minimum hopper angle  
318 ( $\theta_m$ ) and the minimum outlet diameter ( $D_m$ ) are determined based on the powder flow  
319 properties. By using the set of Eqs. (1) to (10) and the values of  $\delta$  and  $\phi_w$  (Table 2), it is  
320 possible to obtain  $\theta_m$  and the hopper flow factor ( $ff$ ) for each SCG sample as shown in Table  
321 3.

322 The results of  $\theta_m$  are in line with expectations, and the general trend is that the worse the  
323 samples' flow properties are, the greater is the hopper inclination to achieve a mass-flow  
324 discharge of SCGs. For example, more inclined hoppers (lower  $\theta_m$ ) are required to make  
325 sample C<sub>100</sub> flow compared to those required for coarser samples A<sub>100</sub> and B<sub>100</sub>; Moreover,  
326 increasing the moisture content of sample C<sub>100</sub> from a dry powder to around 60% drops  $\theta_m$  in  
327 almost 30%, from 14.1 to 9.9°. The  $ff$  is a function of the hopper design and its trend followed  
328 the  $\theta_m$  behavior, as shown in Table 3, with lower values of  $ff$  as the sample flow attributes  
329 worsen.

330 A common rule of thumb used to achieve mass-flow discharge with powders of  
331 unknown flow properties consists of using  $\theta_m = 20^\circ$ , however, it would not be appropriate to

332 handle the SCG samples analysed, which highlights the impact of the findings of this study.  
 333 In real operations, it is likely that funnel discharge or no-flow of SCGs occur with  $\theta_m = 20^\circ$ ;  
 334 hence, compromising process stability, performance, automation, and safety.

335 **Table 3.** Results of the silo design for dry and wet spent coffee ground samples

SCG Sample	$\theta_m$ (°)	$ff$ (-)	$\sigma_{cr}$ (Pa)	$D_m$ (m)	$D^*$ (m)
A <sub>100</sub>	17.0	1.43	-1266	-	0.02
A <sub>100</sub> <sup>20%</sup>	13.6	1.38	-871	-	0.02
A <sub>100</sub> <sup>60%</sup>	15.7	1.37	992	0.57	-
B <sub>100</sub>	17.0	1.45	-920	-	0.02
B <sub>100</sub> <sup>20%</sup>	13.9	1.40	-1490	-	0.02
B <sub>100</sub> <sup>60%</sup>	13.7	1.35	1351	0.83	-
C <sub>100</sub>	14.1	1.42	509	0.40	-
C <sub>100</sub> <sup>20%</sup>	11.6	1.39	-271	-	0.59
C <sub>100</sub> <sup>60%</sup>	9.9	1.23	1333	1.00	-
A <sub>90</sub> C <sub>10</sub>	18.4	1.43	-718	-	0.06
A <sub>80</sub> C <sub>20</sub>	17.1	1.41	-715	-	0.10
B <sub>90</sub> C <sub>10</sub>	15.6	1.43	-1024	-	0.06
B <sub>80</sub> C <sub>20</sub>	17.0	1.45	-683	-	0.10

336 Additionally to the cone angle limitation, for sample C<sub>100</sub> and the ones with 60% of  
 337 moisture content, a minimum hopper diameter ( $D_m$ ) is required to prevent the formation of  
 338 cohesive arches (see case iii, Section 2.4). As shown in Table 3,  $D_m$  increases as the particle  
 339 size decreases, thus sample C<sub>100</sub><sup>60%</sup> has the highest  $D_m$  followed by B<sub>100</sub><sup>60%</sup> and A<sub>100</sub><sup>60%</sup>.

340 For the other SCG samples, the intersection between  $ff$  and  $FF$  is classified as case ii  
 341 (Section 2.4), which means that the powders might flow for any outlet diameter according to  
 342 Jenike's theory because the hopper wall inclination is enough to break up cohesive arches.  
 343 Therefore, in these cases, the outlet diameter is usually set to avoid interlocking effects, with  
 344  $D^*$  equal to 12 times the size of the largest particle. Nevertheless, since even the bigger SCG

345 sample diameter is smaller than 1 mm, the range for  $D^*$  would be 0.66-0.44 cm, which is far  
346 from reasonable for industrial operations.

347 In the literature, there are some examples of  $D_m$  that were proposed based on the  
348 author's handling experience for specific powders rather than with the previous rule of thumb.  
349 In this way, a more conservative design for the outlet diameter of some SCG samples,  
350 denoted by the symbol  $D^*$  in Table 3, might be based on the following premises:

- 351 -  $D^*$  of sample  $C_{100}^{20\%}$  was obtained by linearly interpolating  $D_m$  of samples  $C_{100}$  and  
352  $C_{100}^{60\%}$  concerning the moisture content reported in Table 1;
- 353 - Sample  $B_{100}$  and one with 30% of moisture content presented stable discharge from  
354 silo hoppers of  $\theta_m=30^\circ$  and  $D_m=2.1$  cm in a previous study (Massaro Sousa and  
355 Ferreira, 2020a). Therefore,  $D^*=2.1$  cm was set for samples  $B_{100}$ , and  $B_{100}^{20\%}$ ,  
356 however, without assertiveness on whether it is a mass- or funnel-flow discharge. As  
357 samples  $A_{100}$  and  $A_{100}^{20\%}$  have similar flow properties than  $B_{100}$ , and  $B_{100}^{20\%}$ , the  
358 same  $D^*$  was set to these powders.
- 359 -  $D^*$  of samples  $A_{90}C_{10}$ ,  $A_{80}C_{20}$ ,  $B_{90}C_{10}$ , and  $B_{80}C_{20}$  were obtained based on a  
360 weighted average of  $D_m$  of samples  $A_{100}$  and  $C_{100}$  with respect to the fraction of  
361 fines in the mixture.

362 It should be noted that the reported values for  $D_m$  vary  $\pm 0.5\%$  and  $1.3\%$  by considering  
363 the upper and lower limits of the averaged  $\delta$  and  $\phi_w$  shown in Table 2, respectively.  
364 Meanwhile,  $\theta_m$  vary  $0.5\%$  and  $9.0\%$  in the same range of variation for  $\delta$  and  $\phi_w$ . In the next  
365 section, the effect of variations on the main parameters used for determining  $\theta_m$  and  $D_m$  are  
366 discussed in detail.

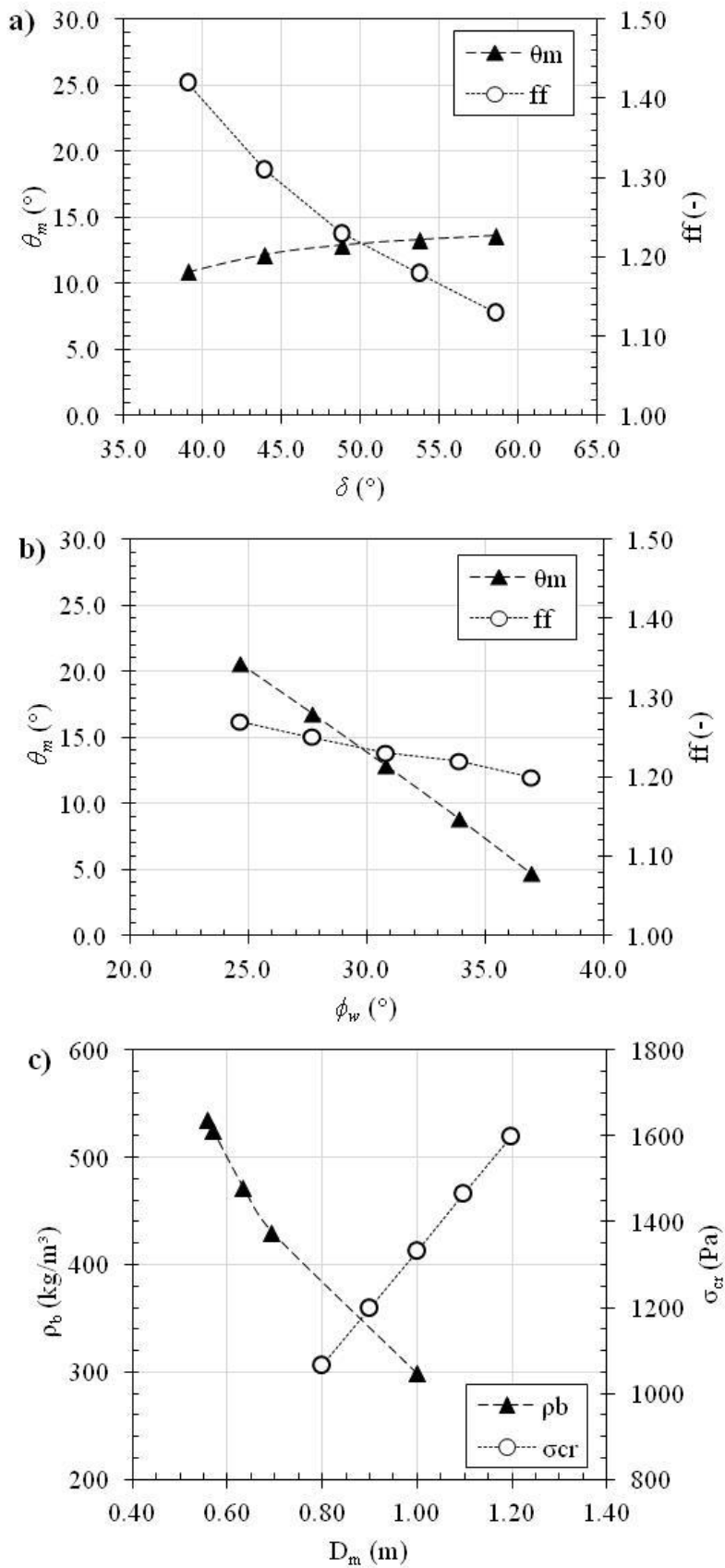
### 367 3.6 Sensitivity of hopper design for SCGs

368 The particle-size distribution and moisture level of spent coffee grounds are not  
369 controlled in industrial processes due to its residue-based nature. Thus, there is some

370 variability on samples' flow and bulk properties, as illustrated in the previous sections, which  
371 ultimately might affect the design of hoppers for the mass-flow discharge of these biomass  
372 powders.

373 The effect of  $\delta$  and  $\phi_w$  on the minimum hopper half-angle and hopper flow factor is  
374 depicted in Fig. 4a and 4b, respectively. Overall,  $\theta_m$  is mainly affected by variations in  $\phi_w$ , and  
375 steeper hoppers are required to achieve mass flow discharge of powders with higher  $\phi_w$ . On  
376 the other hand,  $ff$  is mostly affected by  $\delta$  following an inversely proportional linear  
377 relationship. For intersections between  $ff$  and  $FF$  classified as the case i (Section 2.4), it  
378 means that samples with lower values of  $\delta$  have greater  $ff$  and  $\sigma_{cr}$ , which leads to wider outlet  
379 diameters required to achieve mass-flow discharge of solids from the hopper.

380 Finally, in Fig. 4c it is shown that both the bulk density and  $\sigma_{cr}$  (or implicitly  $FF$ ) play a  
381 major role in the calculated outlet hopper diameter. For example, for intersections between  $ff$   
382 and  $FF$  classified as case i (Section 2.4), the lower is the  $FF$  (i.e. powders with worse  
383 flowability) the higher is  $\sigma_{cr}$ ; hence, wider hopper diameters are required to achieve the mass-  
384 flow discharge of SCGs. Furthermore, higher is the bulk density at the cone outlet, the smaller  
385 is the required hopper diameter size for the gravity-driven, mass-flow discharge of solids. As  
386 shown in Section 3.3, Eqs. (12) to (14) provide a reliable estimation of the bulk density for  
387 dry and wet SCGs under different normal pressures; hence, these equations coupled to  
388 Jenike's method are useful to meet specific requirements for silos with SCGs in the pilot and  
389 industrial-scale plants, as well for improving automation and process monitoring.



390  
 391 **Fig. 4.** Hopper flow factor ( $ff$ ) and hopper half-angle ( $\theta_m$ ) with respect to variations in a)  $\delta$  and  
 392 b)  $\phi_w$ , as well as hopper diameter response to changes in c)  $\rho_b$  and  $\sigma_{cr}$

## 393 **4 Conclusions**

394 This study corroborates that the mean particle diameter and moisture content play an  
395 important role in both bulk properties and flow attributes of SCGs, hence impacting the  
396 design of silo hoppers for the effective mass-flow discharge of powders. Flowability of SCGs  
397 deteriorated with decreasing particle-size and increasing moisture content.

398 From the practical point of view, silo hoppers with inclination and outlet diameter  
399 between  $9.9^\circ$  to  $17.1^\circ$ , and 0.40 to 1.00 m are sufficient to handle most SCG powders. It is  
400 also shown that a densification equation can be coupled to Jenike's method, which might  
401 facilitate the further design of silo hoppers for SCGs with different properties.

402 The findings are valuable for solid-waste researchers and practitioners aiming at the  
403 effective handling of SCGs. Future research could address the design of hoppers for other  
404 relevant food wastes with different material properties, as well as numerical simulations to  
405 investigate particle segregation effects on the hopper discharge for waste biomass powders.

## 406 **Acknowledgements**

407 The authors would like to thank the São Paulo Research Foundation (2016/25946-2 and  
408 2018/11031-8), CNPq (114863/2018-0) and CAPES (Finance code 001) for financial support,  
409 as well as Prof. Dr. Diego Barletta (Università Degli Studi di Salerno/ Italy) for the valuable  
410 discussions concerning the hopper design method.

## 411 **Nomenclature**

<i>A</i>	Parameter calculated as per Eq. (8) (-)
<i>a</i>	Empirical parameter in Eq. (11) (-)
<i>B</i>	Parameter calculated as per Eq. (9) (-)
<i>b</i>	Empirical parameter in Eq. (11) (-)
<i>C</i>	Parameter calculated as per Eq. (10) (-)
<i>c</i>	Cohesion (kPa)
<i>D</i>	Relative density (-)
<i>D<sub>bl</sub></i>	Relative density at loose bulk condition (-)
<i>D<sub>m</sub></i>	Jenike's minimum hopper outlet size (m)
<i>D*</i>	Empirical minimum hopper outlet size (m)

$d_v$	De Brouckere mean diameter ( $\mu\text{m}$ )
$ff$	Hopper flow factor line (-)
$FF$	Flow function (-)
$g$	Gravity acceleration ( $\text{m}\cdot\text{s}^{-2}$ )
$H(\theta_m)$	Parameter calculated as per Eq. (4) (-)
$HR$	Hausner ratio (-)
$MC$	Moisture content (% w.b.)
$MCS$	Major consolidating stress (kPa)
$N$	Consolidating pressure (kPa)
$UYS$	Unconfined yield strength (kPa)
$X$	Parameter calculated as per Eq. (6) (-)
$Y$	Parameter calculated as per Eq. (7) (-)

#### *Greek symbols*

$\beta$	Parameter calculated as per Eq. (2) ( $^\circ$ )
$\rho_b$	Bulk density ( $\text{kg}\cdot\text{m}^{-3}$ )
$\rho_{bl}$	Loose bulk density ( $\text{kg}\cdot\text{m}^{-3}$ )
$\rho_{bc}$	Consolidated bulk density ( $\text{kg}\cdot\text{m}^{-3}$ )
$\rho_s$	Solid density ( $\text{kg}\cdot\text{m}^{-3}$ )
$\phi_w$	Wall friction angle ( $^\circ$ )
$\theta_m$	Jenike's minimum hopper half angle ( $^\circ$ )
$\sigma$	Angle of internal friction ( $^\circ$ )
$\sigma_{cr}$	Critical applied stress (Pa)
$\delta$	Effective angle of internal friction ( $^\circ$ )

#### 412 **References**

- 413 Al-Hamamre, Z., Foerster, S., Hartmann, F., Kröger, M., Kaltschmitt, M., 2012. Oil extracted  
414 from spent coffee grounds as a renewable source for fatty acid methyl ester  
415 manufacturing. *Fuel* 96, 70–76.
- 416 American Society for Testing Material, 2015. Standard test method for shear testing of  
417 powders using the freeman technology FT4 powder rheometer shear cell. ASTM D7891-  
418 15.
- 419 Arnold, P.C., McLean, A.G., 1976. Improved analytical flowfactors for mass-flow hoppers.  
420 *Powder Technol.* 15, 279–281.
- 421 Baião, D.B., Machado, C.S., Condotta, R., 2018. Bidisperse mixtures of sand: effects of  
422 granulometry on its packing and flowability. *J. Eng. Exact Sci.* 04, 117–126.



423 Ballesteros, L.F., Ramirez, M.J., Orrego, C.E., Teixeira, J.A., Mussatto, S.I., 2017.  
424 Optimization of autohydrolysis conditions to extract antioxidant phenolic compounds  
425 from spent coffee grounds. *J. Food Eng.* 199, 1–8.

426 Ballesteros, L.F., Teixeira, J.A., Mussatto, S.I., 2014. Chemical, functional, and structural  
427 properties of spent coffee grounds and coffee silverskin. *Food Bioprocess Technol.* 7,  
428 3493–3503.

429 Barletta, D., Berry, R.J., Larsson, S.H., Lestander, T.A., Poletto, M., Ramírez-Gómez, Á.,  
430 2015. Assessment on bulk solids best practice techniques for flow characterization and  
431 storage/handling equipment design for biomass materials of different classes. *Fuel*  
432 *Process. Technol.* 138, 540–554.

433 Brazinha, C., Cadima, M., Crespo, J.G., 2015. Valorisation of spent coffee through membrane  
434 processing. *J. Food Eng.* 149, 123–130.

435 Campos-Vega, R., Loarca-Piña, G., Vergara-Castañeda, H.A., Oomah, B.D., 2015. Spent  
436 coffee grounds: a review on current research and future prospects. *Trends Food Sci.*  
437 *Technol.* 45, 24–36.

438 Castellanos, A., 2005. The relationship between attractive interparticle forces and bulk  
439 behaviour in dry and uncharged fine powders. *Adv. Phys.* 54, 263–376.

440 Chen, P., Yuan, Z., Shen, X., Zhang, Y., 2012. Flow properties of three fuel powders.  
441 *Particuology* 10, 438–443.

442 Coelho, G.O., Batista, M.J.A., Ávila, A.F., Franca, A.S., Oliveira, L.S., 2021. Development  
443 and characterization of biopolymeric films of galactomannans recovered from spent  
444 coffee grounds. *J. Food Eng.* 289, 110083.

445 Condotta, R., 2017. *Coulabilité des poudres cohesives*. Press. Académiques Francoph.

446 Dai, J., Cui, H., Grace, J.R., 2012. Biomass feeding for thermochemical reactors. *Prog.*  
447 *Energy Combust. Sci.* 38, 716–736.

448 Enstad, G., 1975. On the theory of arching in mass flow hoppers. *Chem. Eng. Sci.* 30, 1273–  
449 1283.

450 Fitzpatrick, J.J., Barringer, S.A., Iqbal, T., 2004. Flow property measurement of food powders  
451 and sensitivity of Jenike’s hopper design methodology to the measured values. *J. Food*  
452 *Eng.* 61, 399–405.

453 Gómez-de la Cruz, F.J., Cruz-Peragón, F., Casanova-Peláez, P.J., Palomar-Carnicero, J.M.,  
454 2015. A vital stage in the large-scale production of biofuels from spent coffee grounds:  
455 The drying kinetics. *Fuel Process. Technol.* 130, 188–196.

456 Ilic, D., Williams, K., Farnish, R., Webb, E., Liu, G., 2018. On the challenges facing the  
457 handling of solid biomass feedstocks. *Biofuels, Bioprod. Biorefining* 12, 187–202.

458 International Coffee Organization, 2019. World Coffee Consumption [WWW Document].  
459 URL <http://www.ico.org/> (accessed 11.15.19).

460 Jenike, A.W., 1964. Storage and flow of solids. *Bull.* 163.

461 Karmee, S.K., 2018. A spent coffee grounds based biorefinery for the production of biofuels,  
462 biopolymers, antioxidants and biocomposites. *Waste Manag.* 72, 240–254.

463 Kawakita, K., Lüdde, K.H., 1971. Some considerations on powder compression equations.  
464 *Powder Technol.* 4, 61–68.

465 Kelkar, S., Saffron, C.M., Chai, L., Bovee, J., Stuecken, T.R., Garedew, M., Li, Z., Kriegel,  
466 R.M., 2015. Pyrolysis of spent coffee grounds using a screw-conveyor reactor. *Fuel*  
467 *Process. Technol.* 137, 170–178.

468 Kondamudi, N., Mohapatra, S.K., Misra, M., 2008. Spent coffee grounds as a versatile source  
469 of green energy. *J. Agric. Food Chem.* 56, 11757–11760.

470 Marinelli, J., Carson, J.W., 1992. Solve solids flow problems in bins, hoppers, and feeders.  
471 *Chem. Eng. Prog.* 88, 22–28.

472 Massaro Sousa, L., Ferreira, M.C., 2020a. Analysis of the Performance of an L-Valve

473 Feeding Spent Coffee Ground Powders into a Circulating Fluidized Bed. *Powder*  
474 *Technol.* 362, 759–769.

475 Massaro Sousa, L., Ferreira, M.C., 2020b. On the Performance of a Spouted Bed type Device  
476 for Feeding Spent Coffee Grounds to a Circulating Fluidized Bed Reactor. *Chem. Eng.*  
477 *Res. Des.* 160, 31–38.

478 Massaro Sousa, L., Ferreira, M.C., 2019a. Spent coffee grounds as a renewable source of  
479 energy: An analysis of bulk powder flowability. *Particuology* 43, 92–100.

480 Massaro Sousa, L., Ferreira, M.C., 2019b. Densification behavior of dry spent coffee ground  
481 powders: Experimental analysis and predictive methods. *Powder Technol.* 357, 149–157.

482 Massaro Sousa, L., Ferreira, M.C., Hou, Q.F., Yu, A.B., 2020a. Feeding Spent Coffee Ground  
483 Powders with a Non-Mechanical L-valve: Experimental Analysis and TFM Simulation.  
484 *Powder Technol.* 360, 1055–1066.

485 Massaro Sousa, L., Ferreira, M.C., Hou, Q.F., Yu, A.B., 2020b. Feeding Spent Coffee  
486 Grounds into Reactors: TFM Simulation of a Non-Mechanical Spouted Bed Type  
487 Feeder. *Waste Manag.* 109, 161–170.

488 McNutt, J., He, Q., 2019. Spent coffee grounds: A review on current utilization. *J. Ind. Eng.*  
489 *Chem.* 71, 78–88.

490 Murthy, P.S., Naidu, M.M., 2012. Production and application of xylanase from *Penicillium*  
491 *sp.* utilizing coffee by-Products. *Food Bioprocess Technol.* 5, 657–664.

492 Mussatto, S.I., Machado, E.M.S., Martins, S., Teixeira, J.A., 2011. Production, composition,  
493 and application of coffee and its industrial residues. *Food Bioprocess Technol.* 4, 661–  
494 672.

495 Oginni, O., Fasina, O., 2018. Theoretical estimation of silo design parameters for fractionated  
496 loblolly pine grinds – Moisture content and particle size effects. *Ind. Crops Prod.* 123,  
497 379–385.

498 Ramírez-Gómez, A., 2016. Research needs on biomass characterization to prevent handling  
499 problems and hazards in industry. *Part. Sci. Technol.* 34, 432–441.

500 Rocha, T.A.F., Ferreira, M.C., Freire, J.T., 2021. Processing spent coffee ground powders for  
501 renewable energy generation: Mechanical dewatering and thermal drying. *Process Saf.*  
502 *Environ. Prot.* 146, 300–311.

503 Salehi, H., Poletto, M., Barletta, D., Larsson, S.H., 2019. Predicting the silo discharge  
504 behavior of wood chips - A choice of method. *Biomass and Bioenergy* 120, 211–218.

505 Silva, M.A., Nebra, S.A., Machado Silva, M.J., Sanchez, C.G., 1998. The use of biomass  
506 residues in the Brazilian soluble coffee industry. *Biomass and Bioenergy* 14, 457–467.

507 Thiagamani, S.M.K., Nagarajan, R., Jawaid, M., Anumakonda, V., Siengchin, S., 2017.  
508 Utilization of chemically treated municipal solid waste (spent coffee bean powder) as  
509 reinforcement in cellulose matrix for packaging applications. *Waste Manag.* 69, 445–  
510 454.

511 Tun, M.M., Raclavská, H., Juchelková, D., Růžičková, J., Šafář, M., Štrbová, K., Gikas, P.,  
512 2020. Spent coffee ground as renewable energy source: Evaluation of the drying  
513 processes. *J. Environ. Manage.* 275, 111204.

514 United Nations, 2019. World population prospects: Highlights [WWW Document]. Dep.  
515 Econ. Soc. Aff. Popul. Div. URL [www.ncbi.nlm.nih.gov/pubmed/12283219](http://www.ncbi.nlm.nih.gov/pubmed/12283219)

516 Voora, V., Bermúdez, S., Larrea, C., 2019. Sustainable Commodities Marketplace Series -  
517 Global Market Report: Coffee [WWW Document]. URL  
518 <https://www.iisd.org/publications/global-market-report-coffee>

519